SEPTEMBER 01 1997

Sound generation by interaction of two inviscid two-dimensional vortices

S. K. Tang; N. W. M. Ko

J. Acoust. Soc. Am. 102, 1463–1473 (1997)
https://doi.org/10.1121/1.420061

Sound generation by interaction of two inviscid two-dimensional vortices

S. K. Tang
Department of Building Services Engineering, The Hong Kong Polytechnic University, Hong Kong

N. W. M. Ko[a)]
Department of Mechanical Engineering, The University of Hong Kong, Hong Kong

(Received 8 November 1995; revised 16 April 1997; accepted 28 April 1997)

Sound generated by the pairing of two inviscid finite-core-size two-dimensional vortices is studied numerically using the contour dynamics method and vortex sound theory. Results indicate that the resulting sound field is a lateral quadrupole type and its axis rotates with nonuniform speed about the origin of the source region. Results also show that the accelerating and decelerating motions of the vortices are important in the sound generation. © *1997 Acoustical Society of America.* [S0001-4966(97)03708-9]

PACS numbers: 43.28.Ra, 43.28.Py, 43.50.Nm [LCS]

INTRODUCTION

The theories of Lighthill[1] and Curle[2] show that sound can be generated by unsteady turbulent flow. In the low Mach number case, the results of Powell[3] and Howe[4] show that the unsteady motion of vorticity is important in sound generation. Studies of vortex sound are, therefore, important in understanding the sound generation of flow noise problems. Typical examples of such problems are jet noise,[5] boundary layer noise,[6] and noise generated from helicopters.[7] Scaling laws for turbulent flow sound intensity have been proposed and some comparisons with experimental results have also been done (for instance, Lush[8]). However, studies, which explicitly relate the sound generation mechanism to vortex motion, are very limited, though a detailed discussion on aerodynamic noise generation is given by Crighton.[9]

It is now well known that sound is generated when two vortices interact. In an axisymmetric low Mach number jet, noise is generated by the pairing of vortex rings.[5] Möhring[10] analytically worked out the sound field generated by the pairing of two thin core closely spaced vortex rings, while Shariff *et al.*[11] computed the sound radiated from inviscid thick core vortex ring pairing using the method of contour dynamics. Tang and Ko[12] showed further that the axial jerk and radial acceleration of the vorticity centroids of the vortex rings play an important role in the pairing noise generation.

In a low Mach number two-dimensional mixing layer and rectangular jet of large-aspect ratio, sound is expected to come from the pairing of two-dimensional vortices. As the near-field source is not compact in this case, the far-field noise is often calculated numerically. For simplicity, the two-dimensional vortices are usually modeled as line vortices during analysis. Recently, Lee and Koo[13] used this technique to compute the sound field pattern generated by two spinning rectilinear vortices in the context of incompressible and inviscid flow. Mitchell *et al.*[14] extended this study to compressible flow. However, they have not addressed the sound generation mechanism involved. In addition, vortices with infinitesimal core sizes are rare in reality. A thick core model appears to be more appropriate for the study and understanding of the mechanism.

In the present study, the sound field generated by the pairing of two equal inviscid thick core two-dimensional vortices is investigated using the method of contour dynamics. Special attention is given to the mechanism of the sound generation. For simplicity, the effect of compressibility is neglected.

I. THEORETICAL AND COMPUTATIONAL CONSIDERATIONS

This section gives brief discussions on the contour dynamics method and vortex sound theory. The two-dimensional pairing noise generation mechanism is also discussed using existing theories.

A. Method of contour dynamics

The shapes of the vortex cores during pairing can be obtained using the method of contour dynamics.[15] This is done by first observing the streamfunction ψ in two dimensions at a point $\mathbf{y}_0$ in the flow field due to a vortex:

$$\psi(\mathbf{y}_0) = -\frac{1}{2\pi}\int\int \omega \ln|\mathbf{y}_0 - \mathbf{y}| dy_1\, dy_2, \tag{1}$$

where y_1 and y_2 denote the longitudinal and transverse coordinates, respectively (Fig. 1). This integration is done across the cross section of the vortex. As $\mathbf{u} = \nabla \times \hat{y}_3\psi$, where y_3 represents the spanwise coordinate and the caret denotes unit vector, use of Stoke's theorem gives the contour integral

$$\mathbf{u}(\mathbf{y}_0) = -\frac{1}{4\pi}\int \omega \ln|\mathbf{y}_0 - \mathbf{y}|^2\, d\mathbf{y} \tag{2}$$

and the singularity in Eq. (2) can be removed by an integration by parts as in Dritschel.[16] Details of the derivation of the method can be found in Zabusky *et al.*[15] and Dritschel.[16] In the present investigation, the node point insertion and relaxation scheme of Pozrikidis and Higdon[17] is used to ensure a

a)Corresponding author. Electronic mail: NWMKO@hkucc.hku.hk

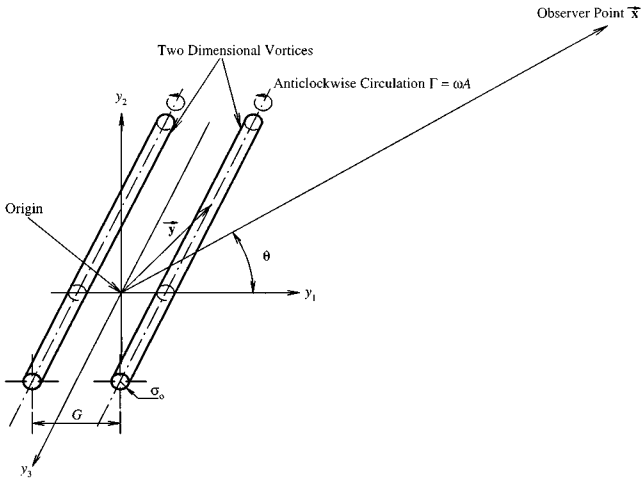

FIG. 1. Schematic diagram of two-dimensional vortices.

smooth contour during the computation. All the contour integrals involved are computed using the four-point Gaussian quadrature procedure and the core shapes are obtained by the fourth-order Runge–Kutta method as in Tang and Ko[12] and Dritschel.[16] The time step is so chosen that no visible difference of results can be found upon its further reduction. The definition of vortex centroid[17] is adopted as

$$\mathbf{y}_c = y_{c1}\hat{y}_1 + y_{c2}\hat{y}_2 = \frac{\int \omega \mathbf{y}\, dA}{\int \omega\, dA}, \tag{3}$$

where $\mathbf{y}_c$ is the position vector of the vortex centroid having the coordinates (y_{c1}, y_{c2}) (see Fig. 2). The velocity, acceleration, and jerk of the vortex in the rest of the paper simply refer to the first, second, and third time derivatives of y_c, respectively. For simplicity, the two vortices are placed symmetrically about the origin at the beginning of the computation. Uniform vorticity within vortex cores is assumed so as to fulfill the requirement of $d\omega/dt = 0$. Under this circumstance, the vortex centroid, as defined by Eq. (3), coincides with the center of mass of the incompressible vortex.

The effect of viscosity on the far-field pressure is not important in the spinning vortex case of Mitchell *et al.*[14] and it is neglected in the present study. Without loss of generality, the vorticity is assumed to be positive (anticlockwise) throughout this study.

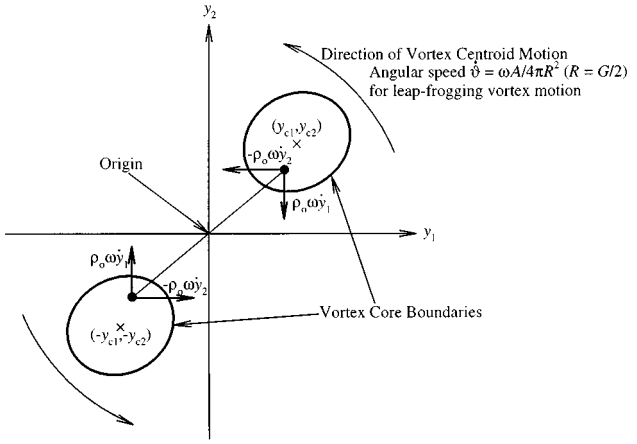

FIG. 2. Forces on core fluids. ×: Vortex centroid.

B. Vortex sound

The sound field from turbulent flow can be obtained by solving the following inhomogeneous wave equation:

$$\frac{1}{c^2}\frac{\partial^2 p}{\partial t^2} - \nabla^2 p = q, \tag{4}$$

where p, c, and t are the far-field pressure, ambient speed of sound, and observer time, respectively. Here, q is the source term, which in the low Mach number case, can be written as $\rho_0 \nabla\cdot(\omega\times\mathbf{u})$, where ω, ρ_0, and $\mathbf{u}$ are vorticity, ambient fluid density, and the velocity of the vorticity propagation, respectively.[3,4] For convenience, boldfaced symbols denote vector quantities in the rest of the paper. Following the method of Möhring,[10] one obtains for a point source of volume dV

$$dp(\mathbf{x},t) = \frac{\rho_0}{12\pi c^2}\frac{\partial^3}{\partial t^3}\frac{(\hat{\mathbf{x}}\cdot\mathbf{y})\mathbf{y}\cdot(\omega\times\hat{\mathbf{x}})}{|\mathbf{x}-\mathbf{y}|}\, dV, \tag{5}$$

where the expression being differentiated is to be evaluated at retarded time $t-|\mathbf{x}-\mathbf{y}|/c$. Here, $\mathbf{x}$ and $\mathbf{y}$ denote, respectively, far- and source-field distances (Fig. 1) and $\hat{\mathbf{x}}$ is an unit vector in the direction $\mathbf{x}$ and is nondimensional. For compact vortex cores, the contribution to the far-field noise from an infinitesimal length dy_3 at $\mathbf{y}$ along a two-dimensional vortex of cross section area A is

$$dp(\mathbf{x},t) = \frac{\rho_0\, dy_3}{12\pi c^2}\frac{\partial^3}{\partial t^3}\left[\frac{1}{|\mathbf{x}-\mathbf{y}|}\left(\cos(2\theta)\int \omega y_1 y_2\, dA + \sin(2\theta)\int \frac{y_2^2 - y_1^2}{2}\,\omega\, dA\right)\right], \tag{6}$$

where θ is the observer angle (Fig. 1). The total far-field pressure $p(\mathbf{x},t)$ generated by the vortices can be obtained by integrating Eq. (6) along y_3:

$$p(\mathbf{x},t) = \frac{\rho_0}{12\pi c^2}\int \frac{1}{|\mathbf{x}-\mathbf{y}|}\frac{\partial^3}{\partial t^3}\left(\cos(2\theta)\int \omega y_1 y_2\, dA + \sin(2\theta)\int \frac{y_2^2 - y_1^2}{2}\,\omega\, dA\right) dy_3. \tag{7}$$

Equation (7) suggests the sound field is a lateral quadrupole. The constant outside the integral in Eq. (7) has no bearing on the sound generation process and is thus ignored in the foregoing discussions. For easy reference, S_1, S_2, D_1, and D_2 are used in the rest of the paper to denote the following integrals:

$$S_1 = \int \omega y_1 y_2\, dA, \quad S_2 = \frac{1}{2}\int \omega(y_2^2 - y_1^2)\, dA,$$
$$D_1 = \int \frac{\dddot{S}_1}{|\mathbf{x}-\mathbf{y}|}\, dy_3, \quad D_2 = \int \frac{\dddot{S}_2}{|\mathbf{x}-\mathbf{y}|}\, dy_3. \tag{8}$$

S_1 and S_2 can be computed using contour integrals and Stoke's theorem. The triple overdot denotes triple time de-

rivative. D_1 and D_2, which are referred as the far-field quadrupole strengths in the rest of the paper, are calculated using the procedure of Ffowcs Williams and Hawkings.[18] They observed that these integrals can be transformed into time integrals by replacing y_3 by a variable t' and because of the singularity at $t' = t - r/c$, one obtains

$$D_i = \int_{-\infty}^{\infty} \frac{\dddot{S}_i(\mathbf{y}, t-|\mathbf{x}-\mathbf{y}|/c)}{|\mathbf{x}-\mathbf{y}|}\, dy_3$$

$$= \int_{-\infty}^{t-r/c} \frac{2c\dddot{S}_i(\mathbf{y}, t')}{\sqrt{c^2(t-t')^2 - r^2}}\, dt'$$

$$\approx \sqrt{\frac{2}{r}} \int_{-\infty}^{t-r/c} \frac{c\dddot{S}_i(\mathbf{y}, t')}{\sqrt{c(t-t') - r}}\, dt', \tag{9}$$

where $r^2 = (x_1^2 - y_{c1}^2) + (x_2^2 - y_{c2}^2)$ and $i = 1,2$. It should be noted that S_i, are independent of y_3. Equation (9) can be solved numerically by further substituting $c(t - t') - r$ by β^2 with the assumption that there is no sound at $\mathbf{x}$ for $t < r/c$. Therefore, the sound field can be solved provided that the time variations of the terms $\dddot{S}_i$ can be obtained. D_i are also the strengths of the two-dimensional far-field quadrupoles as shown in Eq. (7), while $\dddot{S}_i$ denotes the source strengths [Eq. (8)].

C. Sound generation mechanism

Though Eq. (9) suggests that the quadrupole strength depends on D_1 and D_2, the sound generation mechanism involved is more related to S_1 and S_2. The appearance of the former two integrals are only due to the noncompactness of the source region and thus have nothing to do with the vortex motions, not to say the sound generation mechanism. The sound generation mechanism is therefore discussed with Eq. (6).

Under the assumptions of constant vorticity and incompressible vortex, Eq. (6) shows that the sound radiated to the far field at an observer angle θ equals the third time derivative of the cross product of inertia in the angle $(180° - \theta)$,[19] showing that the deformation of the vortex core is important in the sound generation process. However, it is more realistic to describe the sound generation mechanism in terms of some easily quantified parameters, such as force and acceleration of the vortex centroid,[12] as they are easier to verify experimentally than the core shapes. The following paragraphs show how $\dddot{S}_i$ can be related to the motion of the vortex centroids and describe the physical meanings of the terms involved.

Allowing for nonuniform vorticity distribution within the vortex core, the impulse $\mathbf{I}$ of an individual vortex with finite core size is given by the expression

$$\mathbf{I} = \rho_0 \int \mathbf{y} \times \omega\, dA = -\rho_0 \hat{y}_1 \int y_2 \omega\, dA + \rho_0 \hat{y}_2 \int y_1 \omega\, dA. \tag{10}$$

As the vortices are mirror images of each other, the total impulse of the interacting vortices vanishes but those of the individual vortices are vector quantities in two-dimensional space. The force $\mathbf{F}$ acting on each vortex equals the rate of change of impulse of the vortex and thus

$$\mathbf{F} = \frac{d\mathbf{I}}{dt} = -\rho_0 \hat{y}_1 \int \dot{y}_2 \omega\, dA + \rho_0 \hat{y}_2 \int \dot{y}_1 \omega\, dA, \tag{11}$$

where the overdot represents differentiation with respect to time. The forces acting on a small mass of fluid within the vortex cores are illustrated in Fig. 2. Equations (10) and (11) show that the total force acting on the core fluids can be estimated by finding the velocity of the vortex centroids when ω is constant. Also, the conservation of angular momentum J requires that

$$\frac{dJ}{dt} = 0 \Rightarrow \frac{d}{dt} \int \omega(y_1^2 + y_2^2) dA = 0. \tag{12}$$

Besides, the sound energy radiated is negligible compared to the flow energy, especially in the low Mach number case.[1] The total kinetic energy per unit length of the two-dimensional flow K remains fairly constant and thus, following the work of Lamb,[20]

$$\frac{dK}{dt} = 0 \Rightarrow \rho_0 \frac{d}{dt} \int (\dot{y}_1 y_2 - \dot{y}_2 y_1) \omega\, dA = 0. \tag{13}$$

Recalling Eq. (6), one obtains together with Eqs. (12) and (13) that

$$\frac{\partial^3 S_1}{\partial t^3} = \frac{\partial^3}{\partial t^3} \int \omega y_1 y_2\, dA$$

$$= \frac{\partial^2}{\partial t^2} \int \omega(y_1 \dot{y}_2 + y_2 \dot{y}_1) dA$$

$$= \frac{\partial^2}{\partial t^2} \int \omega(2y_1 \dot{y}_2 + y_2 \dot{y}_1 - y_1 \dot{y}_2) dA$$

$$= \frac{\partial^2}{\partial t^2} \int 2\omega y_1 \dot{y}_2\, dA \tag{14a}$$

and

$$\frac{\partial^3 S_2}{\partial t^3} = \frac{\partial^3}{\partial t^3} \int \frac{\omega(y_2^2 - y_1^2)}{2} dA$$

$$= \frac{\partial^3}{\partial t^3} \int \frac{\omega(y_2^2 + y_1^2 - 2y_1^2)}{2} dA$$

$$= -\frac{\partial^2}{\partial t^2} \int 2\omega y_1 \dot{y}_1\, dA. \tag{14b}$$

Similarly, one can also show that

$$\frac{\partial^3 S_1}{\partial t^3} = \frac{\partial^2}{\partial t^2} \int 2\omega y_2 \dot{y}_1\, dA$$

and (14c)

$$\frac{\partial^3 S_2}{\partial t^3} = \frac{\partial^2}{\partial t^2} \int 2\omega y_2 \dot{y}_2\, dA.$$

It is observed from Eqs. (10) and (14) that $\partial^3 S_2 / \partial t^3$ represents the total anticlockwise couple about the origin acting on the vortex core fluids (Fig. 2). It is therefore related to the

rotation of the vortex core fluids about the origin. However, one should bear in mind that the total couple acting on the core fluids vanishes because the anticlockwise and clockwise couple balance each other in the present case.

The meaning of $\partial^3 S_1/\partial t^3$ is far less trivial. It is the magnitude of the product of a force and a distance in one direction; either in the y_1 or y_2 direction. As the vortex centroids are rotating anticlockwise about the origin ($\omega > 0$), Eq. (11) shows that the total force acting on one vortex core is always pointing towards the two axes (Fig. 2). Here, $\partial^3 S_1/\partial t^3$ seems to represent somewhat like the ''work done'' in one direction against the displacement of the vortex core fluids from the axis in that direction. Thus sound is generated by the force acting on individual vortex. However, in this two dimensional case, Eq. (14) cannot be further decomposed to relate the sound generation mechanism with the acceleration and jerk of the vortex centroids as explicitly as in the axisymmetric vortex ring case of Tang and Ko,[12] unless the cores are very thin.

In the thin core case, the vortices undergo circular motion with angular speed $\dot{\vartheta} = \omega A/4\pi R^2$, where R is the radius of the circular orbit, which equals to half the separation between vortex centroids G.[3] Thus one can observe that

$$y_{c1} = R\cos(\dot{\vartheta}t) \quad \text{and} \quad y_{c2} = R\sin(\dot{\vartheta}t). \tag{15}$$

For core of infinitesimal size, its deformation is negligible and it can be assumed that the vortex cores remain circular throughout the interaction, Eq. (14) can then be simplified to

$$\begin{aligned}\frac{\partial^3 S_1}{\partial t^3} &= -16AR^2\rho_0(R\dot{\vartheta}^2)^2\cos(2\dot{\vartheta}t)\\ &= 16AR^2\rho_0[(\ddot{y}_{c2})^2-(\ddot{y}_{c1})^2] = E_1,\\ \frac{\partial^3 S_2}{\partial t^3} &= -16AR^2\rho_0(M\dot{\vartheta}^2)^2\sin(2\dot{\vartheta}t)\\ &= -32AR^2\rho_0\ddot{y}_{c1}\ddot{y}_{c2} = E_2,\end{aligned} \tag{16}$$

where E_i represent the source strengths associated with nonlinear coupling of longitudinal and transverse accelerations. Equations (16) also show the importance of the accelerations $\ddot{y}_{c1}$ and $\ddot{y}_{c2}$ in the sound generation in the thin core case. The constant ambient density ρ_0 will be neglected in the rest of the discussion. It should be noted in this nondeformable thin vortex core case that the accelerations $\ddot{y}_{c1}$ and $\ddot{y}_{c2}$ are proportional to the angular speed $\dot{\vartheta}$ and the angular acceleration $\ddot{\vartheta}$ vanishes. When the vortex cores are deformable, $\ddot{y}_{c1}$ and $\ddot{y}_{c2}$ will no longer be proportional to $\dot{\vartheta}$ and $\ddot{\vartheta}$ is time dependent.

The situation in the thick core case is complicated because the vortex core shapes are noncircular and change with time. The angular velocity $\dot{\vartheta}$ and R, therefore, are functions of time so that Eqs. (16) alone are unable to give the sound field. However, R and $\dot{\vartheta}$ for the two vortices are the same as far as their circulations are equal. When the vortex cores are thick, $\dddot{S}_i$ cannot be expressed analytically as in Eqs. (16). It will be shown numerically in the next section that

$$\begin{aligned}\dddot{S}_1 &\approx E_1 + k_1(\dot{y}_{c1}\dot{y}_{c2}r_c\ddot{\theta}_c + \tfrac{1}{2}(\dot{y}_{c1}^2-\dot{y}_{c2}^2)\ddot{r}_c),\\ \dddot{S}_2 &\approx E_2 + k_2(\dot{y}_{c1}\dot{y}_{c2}\ddot{r}_c - \tfrac{1}{2}(\dot{y}_{c1}^2-\dot{y}_{c2}^2)r_c\ddot{\theta}_c),\end{aligned} \tag{17}$$

when the vortices do not coalesce. Here, k_i are constants depending on the separation of the vortex centroids and r_c and θ_c are, respectively, the radial and angular positions of vortex centroid. Therefore, though Eqs. (16) are obtained due to the circular motion characteristics of thin core vortices, E_1 and E_2 are also important in thick core vortex pairing noise generation as far as the vortices do not coalesce. As will further be shown later, numerical data in the case of coalescence favor the following relationships:

$$\begin{aligned}\dddot{S}_1 &\approx \exp(-\omega(t-r/c)/b)(l_{11}\ddot{y}_{c1}+l_{12}\ddot{y}_{c2}),\\ \dddot{S}_2 &\approx \exp(-\omega(t-r/c)/b)(l_{21}\ddot{y}_{c1}+l_{22}\ddot{y}_{c2}),\end{aligned} \tag{18}$$

where b and l_{ij} are constants. Thus the sound generation mechanism in the pairing of two-dimensional thick core vortices involves the accelerating or decelerating motions of the vortex core fluids. The numerical results and the derivation of Eqs. (17) and (18) are given in the next section.

II. NUMERICAL RESULTS

The computations were done on the IBM 9076 Scalable POWERparallel system of The University of Hong Kong. Two types of interactions are considered in this study. The first one is the leapfrogging motion and the other the vortex coalescence.[15] In the former type of interaction, the vortex centroids undergo circular motion. Deformation of the vortex cores occurs at the same time but the degree of deformation is not severe. The latter type of interaction involves severe core deformation together with the formation of strips of vorticity around the interacting vortices. These evolutions of the vortex cores are well known[15,21] and it will not be discussed in detail in the present paper. In the following sections, both the sound field and sound generation mechanism are addressed. In order to differentiate observer time and interaction time, t_i represents vortex interaction time which can also be considered as the sound generation time. Numerically, t_i equals the retarded time, that is $t_i = t - r/c$. It is introduced to differentiate the time scale of vortex interaction and of far-field noise radiation. Also, all quantities, unless otherwise stated, are nondimensionalized in the rest of the paper. Lengths, such as y_{c1} and R, are normalized by σ_0, where σ_0 is the initial core radius (Fig. 1), and times, such as t_i and t, by ω^{-1}. Other quantities presented are normalized by combinations of σ_0 and ω. All velocities and accelerations, except the angular velocity and acceleration, which are normalized by ω and ω^2, respectively, are normalized by $\sigma_0\omega$ and $\sigma_0\omega^2$, respectively. The terms $\dddot{S}_1$, $\dddot{S}_2$, E_1, and E_2 are normalized by $\sigma_0^4\omega^4$, and the quadrupole strengths D_1 and D_2 by $\sigma_0^3\omega^4$.

A. Leapfrogging case

Figure 3 shows the shapes of the initially trailing vortex core for an initial spacing of $G/\sigma_0 = 5$ and angular momentum $J = 21.2$ at time $\omega t_i = 20$, 40, and 60. Leapfrogging motion without severe core formation is observed. The maxi-

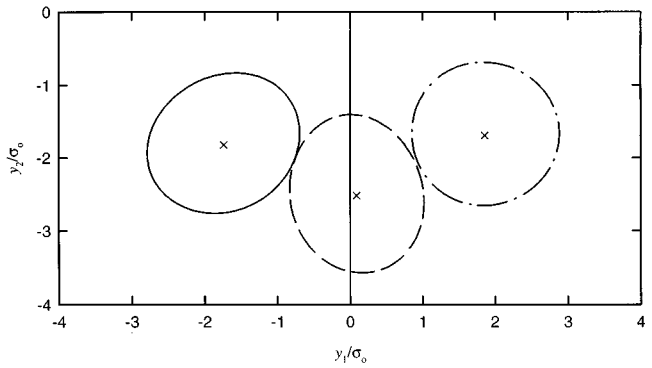

FIG. 3. Variation of initially trailing vortex core shape during interaction. $G/\sigma_0 = 5$, $J = 21.2$. ———: $\omega t_i = 20$; – – –: $\omega t_i = 40$; —·—: $\omega t_i = 60$. ×: Vortex centroid.

mum variations of the cross-sectional area and angular momentum of individual vortices are less than 0.1% and thus it can be assumed that the angular momentum and circulation are conserved. The corresponding time variations of D_1 and D_2 are shown in Fig. 4(a). Wavy oscillations appear on these time variations but the differences between D_1 and D_2 are not only in magnitude but also in phase. As $\ddot{S}_1$ and $\ddot{S}_2$, and thus D_1 and D_2, represent the magnitudes of two independent quadrupoles as shown in Eq. (7), direct summation of these quantities has no physical meaning. The magnitude of the resultant quadrupole $\sqrt{D_1^2+D_2^2}$ also fluctuates with time [Fig. 4(a)]. This shows that the vortex system does not radiate constant sound power. Such radiation depends on the states of the vortices as discussed in the next paragraph. It can be noted that the means of D_1 shown in Fig. 4(a) do not vanish, while that for a far field of any source should be zero. The means are about 9% of the corresponding peak values. It is probably due to the time frame shown in Fig. 4(a) which does not cover a full period of the low-frequency component in the computed far-field sound.

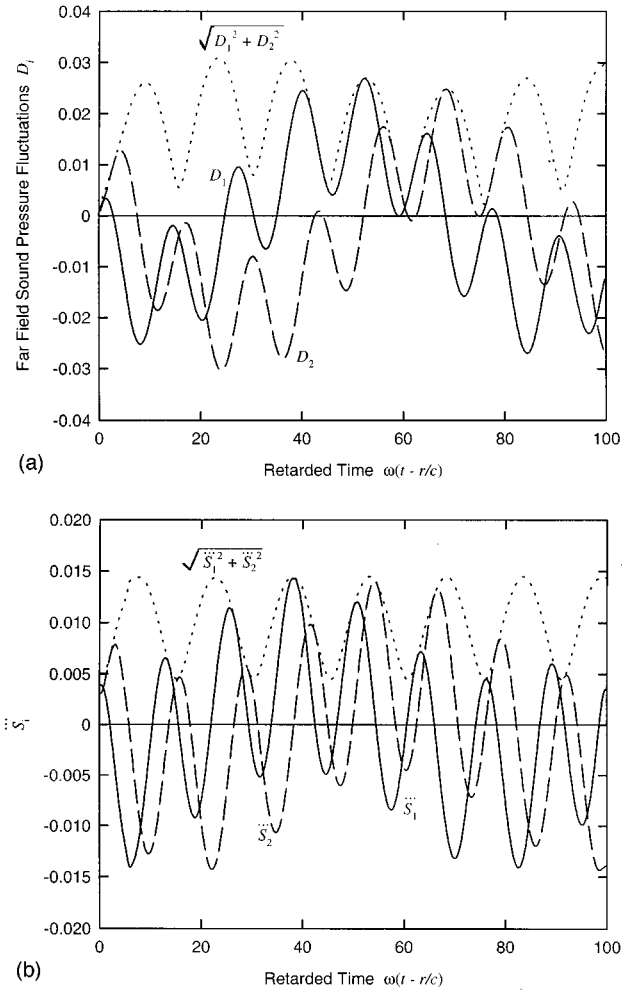

FIG. 4. (a) Time variations of far-field pressure fluctuations during leapfrogging vortex motion. ———: D_1; – –: D_2; ·····: $\sqrt{D_1^2+D_2^2}$. (b) Time variations of $\ddot{S}_i$. ———: $\ddot{S}_1$; – –: $\ddot{S}_2$; ·····: $\sqrt{\ddot{S}_1^2+\ddot{S}_2^2}$.

As $\ddot{S}_1$ and $\ddot{S}_2$ are more related to the generation of sound, their time variations give information on the sound generation process. The corresponding time variations of $\dddot{S}_1$ and $\dddot{S}_2$ are shown in Fig. 4(b). Similar to Fig. 4(a), the means of $\dddot{S}_1$ appear to be nonzero, probably for the same reason as stated before. The mean values in Fig. 4(b) amount to 5% of the corresponding peak values. It can be observed that these time fluctuations contain low- and high-frequency components. The high-frequency wavy oscillations on these time traces have higher magnitudes relative to those of the corresponding low-frequency components than those on D_1 and D_2. This is probably due to the phase difference of the sound waves radiated to the far-field position $\mathbf{x}$ from different elements along the lengths of the vortices, which tends to smooth out large fluctuations. Both the magnitudes of $\dddot{S}_1$ and $\dddot{S}_2$ vary with ω^3, while those of D_1 and D_2 with $\omega^{3.5}$ (not presented here). The latter is consistent with the existing two-dimensional vortex sound theory.[18] $\dddot{S}_1$ and $\dddot{S}_2$ will be further discussed as they are more related to the mechanism of sound generation. The constant phase shift between $\dddot{S}_1$ and $\dddot{S}_2$, and thus between D_1 and D_2, suggests a lateral quadrupole sound field. In addition, the dotted line in Fig. 4(b) illustrates that the amplitude of sound generated by the interaction attains local minima at $\omega(t-r/c)=\omega t_i = 15.2, 30.4, 45.6, \ldots$, while local maxima are observed at $\omega t_i = 7.7, 22.8, 37.7, \ldots$. At these instants, the vortex system is in the most or least efficient state of sound generation. Defining the differential radius $\Delta\sigma$ as the difference between maximum and minimum distances of the elements on the core boundary from the vortex centroid:

$$\Delta\sigma = [\max(|\mathbf{y}-\mathbf{y}_c|) - \min(|\mathbf{y}-\mathbf{y}_c|)]/\sigma_0,$$

where $\mathbf{y}$ is on the boundary of the vortex core, so that $\Delta\sigma = 0$ corresponds to a circular core, Fig. 5 shows that the minimum $\sqrt{\dddot{S}_1^2+\dddot{S}_2^2}$ appears at the instant of small differential radius, suggesting that the vortex system radiates less sound energy when the core shape is close to circular. The degree of deviation of the core from circular shape governs the amplitude of sound generation. However, such deviation cannot be easily quantified.

Figure 6 gives the polar plots of normalized far-field sound-pressure amplitudes $|p|$ obtained from Eq. (7) at $\omega t_i = 20$, 40, and 60. The sound fields are lateral quadrupoles. The axes of the quadrupole rotate with nonuniform angular speed about the origin. The major direction of rotation of the

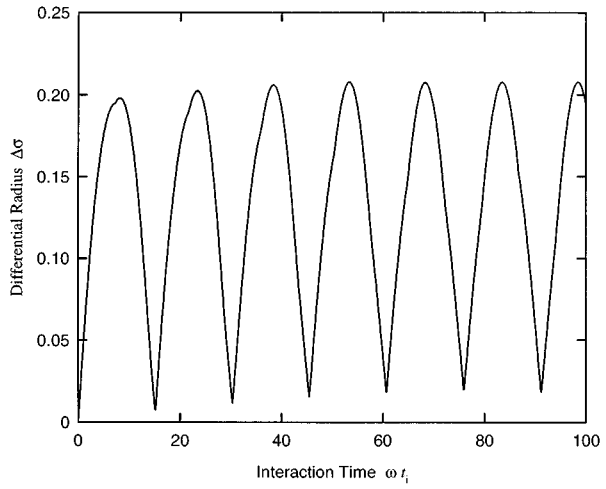

FIG. 5. Time variation of differential radius. $G/\sigma_0 = 5$, $J = 21.2$.

quadrupole is anticlockwise and is the same as that of the vortex field. However, there are instants that the quadrupole is rotating clockwise (Fig. 7). This is different from the thin core vortex pairing results of Powell,[3] Lee and Koo,[13] and Mitchell *et al.*[14] which show that the quadrupole always rotates in the direction of the vortex field. The frequency of the wavy oscillation in $\dddot{S}_1$ and $\dddot{S}_2$ [Fig. 4(b)] is not the same as that in Fig. 7. This will be discussed later.

Though the vortex centroids undergo the type of circular motion described by Eqs. (15) with a mean anticlockwise angular velocity $\dot{\vartheta} = \omega A/4\pi R^2$ and their longitudinal and transverse velocities vary nearly sinusoidally with time (Fig. 8), the corresponding accelerations are not (Fig. 9). This may be due to the nutation or rotation of the deformed vortex core as in the vortex ring pairing case.[11,12] However, the low-frequency time variations of these time traces coincide with those calculated using Eqs. (16) which is developed using a nondeformable thin core assumption. The high-frequency wavy oscillations on the acceleration time traces, which have small magnitudes, seem to come from the fluctuating radial and angular accelerations of the vortex centroids in this thick

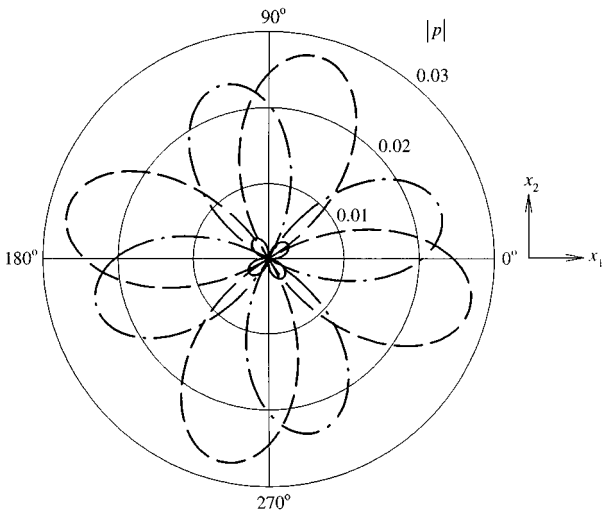

FIG. 6. Polar plot of far-field sound-pressure amplitude. $G/\sigma_0=5$, $J=21.2$. ———: $\omega t_i=20$; – – –: $\omega t_i=40$; —·—: $\omega t_i=60$.

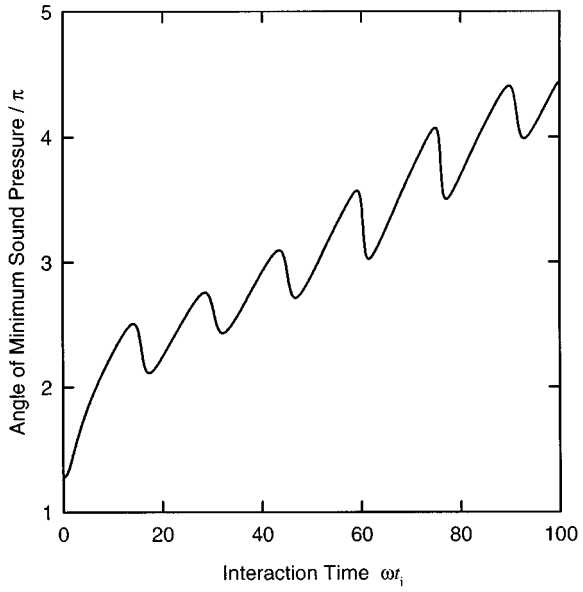

FIG. 7. Time variation of angle of minimum far-field sound pressure. $G/\sigma_0=5$, $J=21.2$.

core case as indicated in Fig. 9. These variations of the radial and tangential accelerations of the vortex centroid, denoted by $\ddot{r}_c$ and $r_c\ddot{\theta}_c$, respectively, are roughly sinusoidal (Fig. 9). For thick core vortices, the high-frequency wavy oscillations on $\dddot{S}_1$ and $\dddot{S}_2$ [Fig. 4(b)] are not expected to come from the linear coupling of velocity and acceleration. Though the magnitudes of the high-frequency wavy oscillations on the radial and tangential acceleration time traces are small (Fig. 9), it will be shown in the next two paragraphs that these oscillations are related to the sound generation process.

The following discussion on the sound generation mechanism for thick core vortex pairing starts from using Eqs. (16). Figures 4(b) and 10 show that the low-frequency components in the source strengths of $\dddot{S}_1$ and $\dddot{S}_2$ can be approximated by E_1 and E_2 given by Eqs. (16), respectively. The time variations of the differences $(\dddot{S}_1 - E_1)$ and $(\dddot{S}_2 - E_2)$ are sinusoidal with period $\omega T = 12.5$ (Fig. 10),

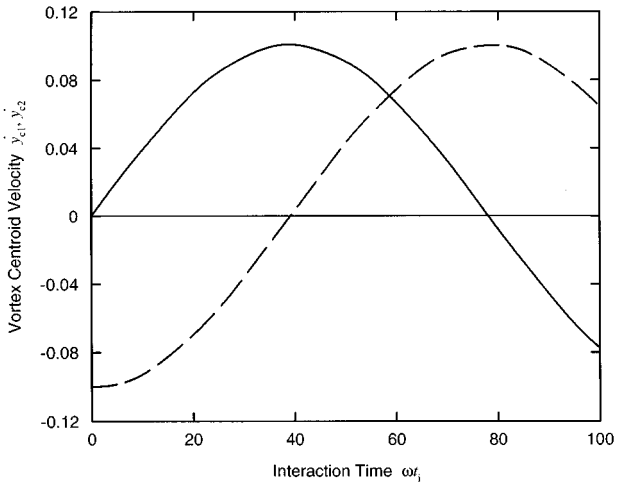

FIG. 8. Time variations of velocities of initially trailing vortex centroid. $G/\sigma_0=5$, $J=21.2$. ———: Longitudinal velocity $\dot{y}_{c1}$; – –: transverse $\dot{y}_{c2}$.

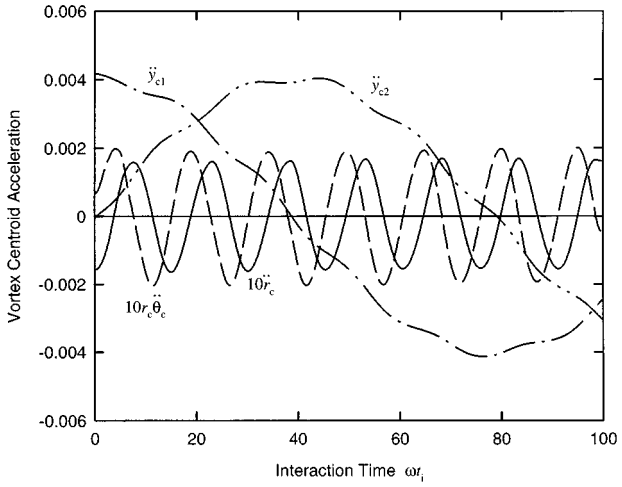

FIG. 9. Time variations of initially trailing vortex centroid accelerations. $G/\sigma_0=5$, $J=21.2$. ———: Radial acceleration $\ddot{r}_c$; – –: tangential acceleration $r_c\ddot{\theta}_c$; —·—: longitudinal acceleration $\ddot{y}_{c1}$; —··—: transverse acceleration $\ddot{y}_{c2}$.

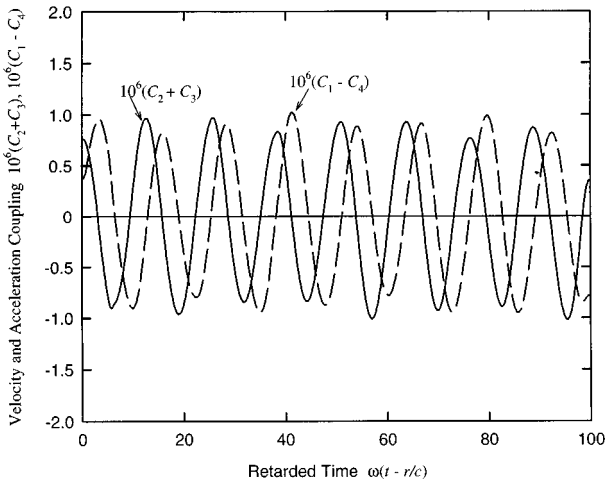

FIG. 11. Time variations of couplings of velocities and accelerations. $G/\sigma_0=5$, $J=21.2$. ———: (C_2+C_3); – –: (C_1-C_4).

which agrees with that of $\dddot{S}_i$ [Fig. 4(b)]. However, it is different from that of the radial or tangential accelerations shown in Fig. 9, indicating that these wavy oscillations are not generated by these two accelerations alone. Some couplings with other dynamical parameters are expected.

As discussed before, it is more rewarding to relate the sound generation mechanism to the physical parameters that describe the motion of the vortices. From the periods of the high-frequency wavy oscillations of $\dddot{S}_1$ and $\dddot{S}_2$ [$\omega T_s\approx 12.5$, Figs. 4(b) and 10], $\ddot{r}_c$ and $r_c\ddot{\theta}_c$ ($\omega T_a\approx 15$, Fig. 9), and the time variations of $\dot{y}_{c1}$ and $\dot{y}_{c2}$ ($\omega T_v\approx 157$, Fig. 8), which contain negligible high-frequency components, it is found that

$$\frac{1}{T_s}\approx\frac{1}{T_a}+\frac{2}{T_v}.$$

This suggests that the wavy oscillations on $\dddot{S}_1$ and $\dddot{S}_2$ are related to the coupling between the radial/tangential acceleration and the second order of longitudinal or radial velocity. The Coriolis acceleration component $2\dot{r}_c\dot{\theta}_c$, which is not shown here, is not relevant as its frequency is double those of the acceleration terms. From the sinusoidal characteristics of these acceleration and velocity terms, four types of couplings can be defined. They are named as C_i, where $i=1$, 2, 3, and 4, as follows:

$$C_1=\dot{y}_{c1}\dot{y}_{c2}\ddot{r}_c,\quad C_2=\dot{y}_{c1}\dot{y}_{c2}r_c\ddot{\theta}_c,$$
$$C_3=\tfrac{1}{2}(\dot{y}_{c1}^2-\dot{y}_{c2}^2)\ddot{r}_c,\quad C_4=\tfrac{1}{2}(\dot{y}_{c1}^2-\dot{y}_{c2}^2)r_c\ddot{\theta}_c. \tag{19}$$

Figures 10 and 11 show that the time variations of (C_3+C_2) and (C_1-C_4) follow closely those of $(\dddot{S}_1-E_1)$ and $(\dddot{S}_2-E_2)$, respectively. Therefore, the following relationships are suggested:

$$\dddot{S}_1\approx E_1+k_1(C_3+C_2)\quad\text{and}\quad\dddot{S}_2\approx E_2+k_2(C_1-C_4). \tag{20}$$

Here, k_1 and k_2 are dimensional constants with unit m^3 but they are effectively the same (not shown here) and are denoted by k in the rest of the discussion. Equations (20) suggest that the pairing sound is related to the nonlinear couplings between accelerations (both longitudinal, transverse, radial, and tangential) and longitudinal and transverse velocities of vortex centroids. Similar phenomenon is observed for other values of initial spacing G/σ_0 as long as vortex coalescence does not occur. However, Eqs. (20) give better approximation as G/σ_0 increases. The value of k can be estimated using the method of least squares. Figure 12 illustrates the error of sound intensity estimation ϵ that is inherent in the approximation for the first expression in Eqs. (20). This error is defined by the expression

$$\epsilon=\int(\dddot{S}_1-E_1-k(C_3+C_2))^2\,dt\Big/\int(\dddot{S}_1)^2\,dt \tag{21}$$

and is thus a measure of the accuracy of using Eqs. (20) for the approximation of source strengths. It is generally less than 12%. The error associated with $\dddot{S}_2$ is very close to that calculated by the above expression and is not discussed. The error increases with decreasing G/σ_0, but the intensity associated with the high frequency wavy oscillations becomes

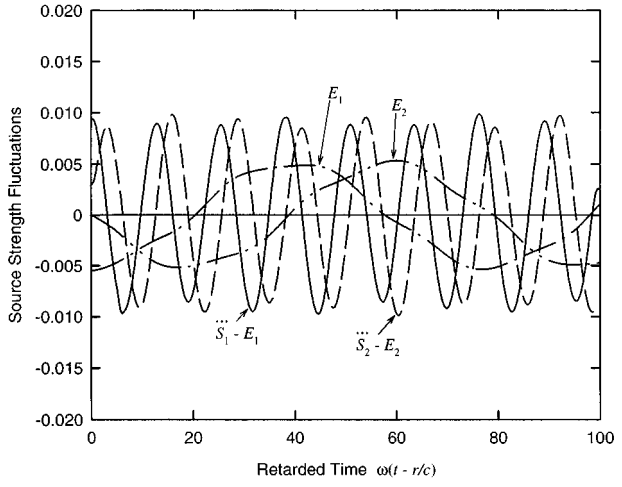

FIG. 10. Time variations of source strengths. $G/\sigma_0=5$, $J=21.2$. ———: $\dddot{S}_1-E_1$; – –: $\dddot{S}_2-E_2$; —·—: E_1; —··—: E_2.

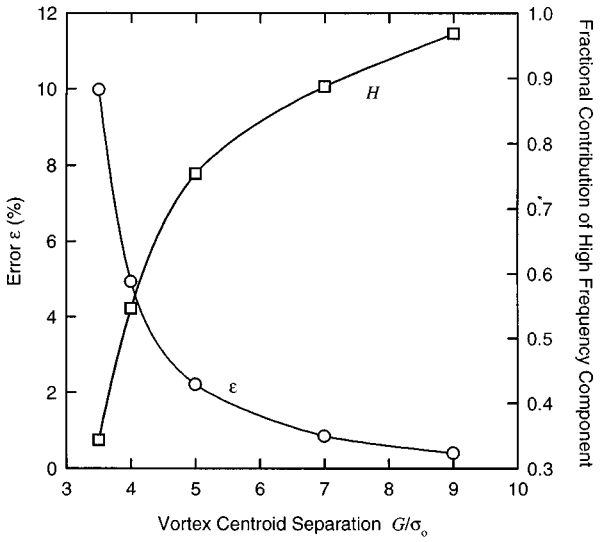

FIG. 12. Error in sound intensity estimation and contribution of high-frequency components in sound radiation. $G/\sigma_0=5$, $J=21.2$. ○: Error in sound intensity estimation by Eq. (21); □: contribution of high-frequency components in overall sound intensity radiation.

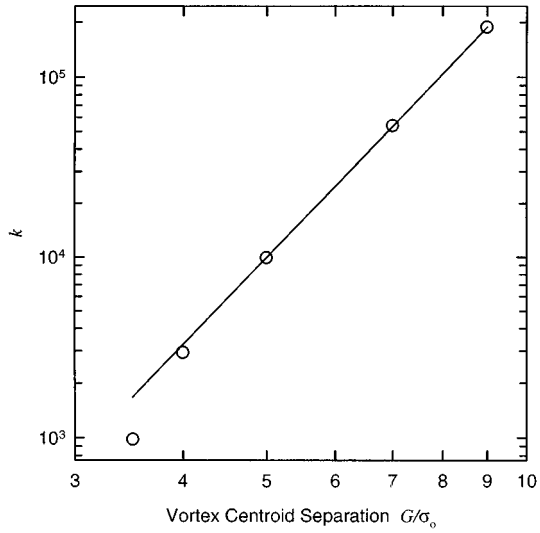

FIG. 13. Variation of proportionity constant k with vortex centroid separation for leapfrogging vortex motion. ○: Numerical data from least-squares method; ———: Eq. (23).

less important for small G/σ_0 (Fig. 12). Results for $G/\sigma_0=3$ will be discussed in the next section, as coalescence occurs at this separation. Defining the fractional contribution of the high-frequency component in the source strength, which reveals the importance of the high-frequency component in the sound generation, as

$$H=\frac{\int k^2(C_3+C_2)^2\,dt}{\int (E_1+k(C_3+C_2))^2\,dt}, \tag{22}$$

it can be observed in Fig. 12 that H increases with G/σ_0 and $H\to 1$ as G/σ_0 becomes large. This shows that the couplings between the radial and tangential accelerations and the longitudinal and transverse velocities are important sources of sound for large G/σ_0 but they become insignificant at small G/σ_0, implying that they are not the main source of sound in the coalescence case. This will be discussed later.

Figure 13 shows that $k\propto(G/\sigma_0)^5$. It can also be estimated from Fig. 13 that

$$k\approx\frac{10}{\pi}\left(\frac{G}{\sigma_0}\right)^5. \tag{23}$$

Equation (23) is included in Fig. 13 and it remains unchanged for other values of ω unless vortex coalescence occurs.

This section shows that the sound generated by the leapfrogging motion of two identical inviscid finite-core-size two-dimensional vortices consists of low-frequency and high-frequency components (Fig. 10). The former is due to the longitudinal and transverse accelerating motions of the vortices, while the latter comes from the coupling of the longitudinal and transverse velocities and the radial and tangential accelerations resulting from the vortex core deformation, showing the importance of the accelerations of vortex centroids in the sound generation mechanism (Fig. 11). Jerk does not appear to be important in this case and this is different from the case of vortex ring pairing.[12]

B. Vortex coalescence case

Figure 14 illustrates the core shapes of the coalescing vortices for $G/\sigma_0=3$, $J=8.36$ at $\omega t_i=30$. The shapes of the two vortex cores are mirror images of each other. The changes in vortex cross-sectional area and angular momentum are again negligible. Serious core deformation is observed and the motion of the vortex centroids is far from circular, as shown in Fig. 15. Also shown in Fig. 15 is that the vortex centroid does not always rotate in anticlockwise direction, resulting in large changes in its angular velocity at the turning point (Fig. 16). Large changes in its radial and angular accelerations are also observed at this instant (Fig. 17). There is a general tendency for decreasing vortex centroid spatial separation at increased interaction time as shown in Fig. 15, which is also observed in vortex ring coalescence.[12] This decrease in vortex centroid separation is accompanied by an increase in the magnitudes of the longitudinal and transverse accelerations (Fig. 17).

The time variations of the source strengths $\dddot{S}_1$ and $\dddot{S}_2$ are

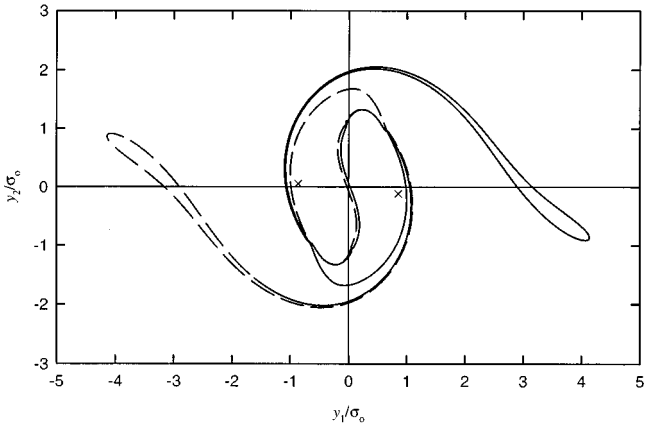

FIG. 14. Vortex core shapes during coalescence. $G/\sigma_0=3$, $J=8.64$. ———: Initially trailing vortex; ––: initially leading vortex. ×: Vortex centroids.

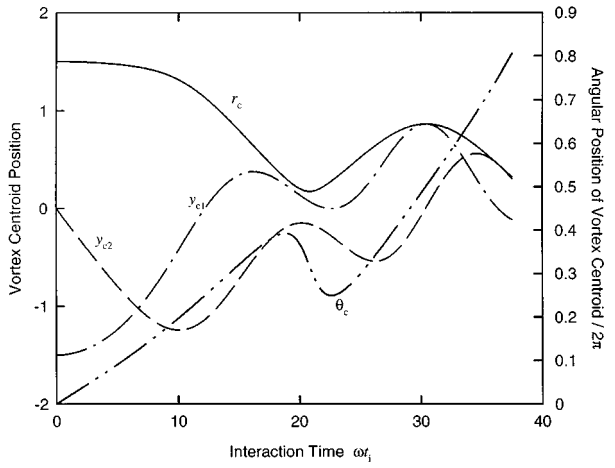

FIG. 15. Time variations of initially trailing vortex centroid positions. $G/\sigma_0 = 3$, $J = 8.64$. ———: r_c; —·—·—: θ_c; – –: y_{c2}; —·—: y_{c1}.

shown in Fig. 18. The rotating quadrupole nature of the sound field and its manner of rotation are similar to those in the previous case and are not discussed again. However, it is observed that the amplitude of the source strengths decreases at increased interaction time during which an overall decrease in the spatial separation between the vortex centroids is observed (Fig. 15), though there is an increase in the magnitudes of vortex centroid accelerations (Fig. 17). The far-field sound in this coalescence case does not seem to contain two components as in the previous leapfrogging case. Also, the magnitude of sound generated does not appear to be directly associated with the degree of vortex core deformation. Local minimum of source strength magnitude $\sqrt{\dddot{S}_1^2+\dddot{S}_2^2}$ appears at $\omega t_i \approx 30$ while the maximum occurs at $\omega t_i \approx 9$ when the vortex core is less severely deformed (not shown here). This indicates that a higher degree of core deformation does not necessarily lead to greater sound radiation in the coalescence case. This is different from the results obtained in the leapfrogging case.

The smooth time variations of the source strengths $\dddot{S}_1$

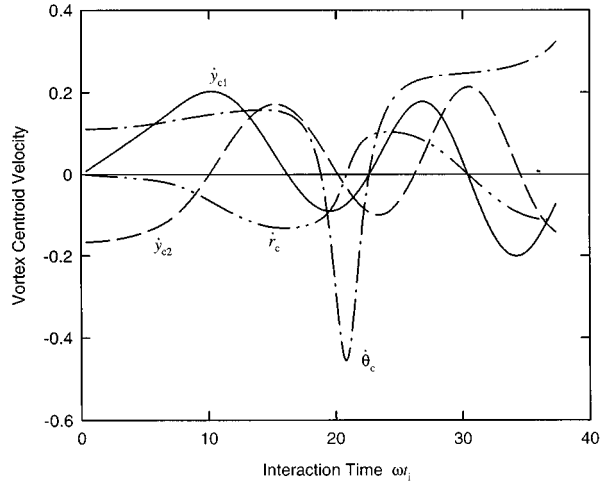

FIG. 16. Time variations of vortex centroid velocities. $G/\sigma_0=3$, $J=8.64$. ———: $\dot{y}_{c1}$; – –: $\dot{y}_{c2}$; —·—: angular velocity $\dot{\theta}_c$; —·—·—: radial velocity $\dot{r}_c$.

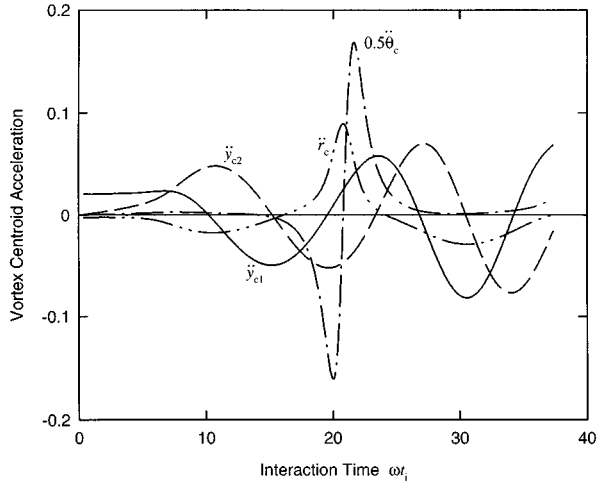

FIG. 17. Time variations of initially trailing vortex accelerations. $G/\sigma_0=3$, $J=8.64$. ———: $\ddot{y}_{c1}$; – –: $\ddot{y}_{c2}$; —·—: angular acceleration $\ddot{\theta}_c$; —·—·—: radial acceleration $\ddot{r}_c$.

and $\dddot{S}_2$ shown in Fig. 18 suggests that the vortex coalescence sound is not much related to the radial acceleration $\ddot{r}_c$ and the tangential acceleration $r_c\ddot{\theta}_c$ (Fig. 17). Their time variation frequencies coincide with those of the longitudinal and transverse velocities ($\dot{y}_{c1}$ and $\dot{y}_{c2}$) and accelerations ($\ddot{y}_{c1}$ and $\ddot{y}_{c2}$) (Figs. 16 and 17). The sound cannot come from the nonlinear couplings of these velocities or accelerations or both, as any such kind of couplings would increase the time variation frequency. Equation (16) is not applicable as the vortex centroids are not in circular motion in this case. The decrease in amplitudes of the source strengths $\dddot{S}_1$ and $\dddot{S}_2$ at increased interaction time suggests the importance of spatial separation in the sound generation mechanism as it is the only quantity that relates to vortex motion and shows a definite decreasing trend. The longitudinal and transverse velocities are not generally believed to be important in the generation of vortex sound, otherwise sound can be generated by steady vortex motion. However, they may affect the amplitude of the radiated sound. Thus it is expected that sound is generated by the longitudinal and transverse accelerating motions of the vortex centroids.

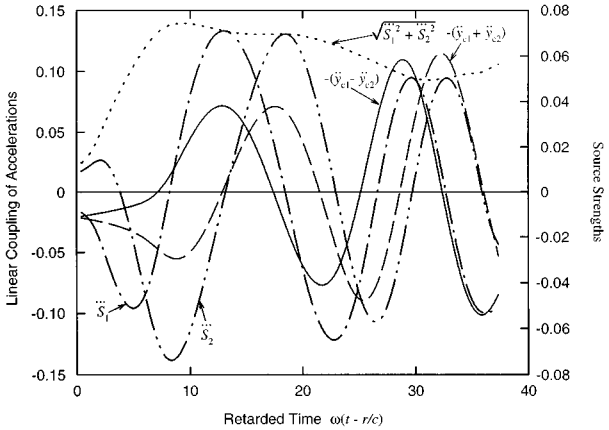

FIG. 18. Time variations of source strengths and linear couplings of accelerations. $G/\sigma_0=3$, $J = 8.64$. ———: $-(\ddot{y}_{c1} - \ddot{y}_{c2})$; – –: $-(\ddot{y}_{c1} + \ddot{y}_{c2})$; —·—: $\dddot{S}_1$; —·—·—: $\dddot{S}_2$; ·····: $\sqrt{\dddot{S}_1^2+\dddot{S}_2^2}$.

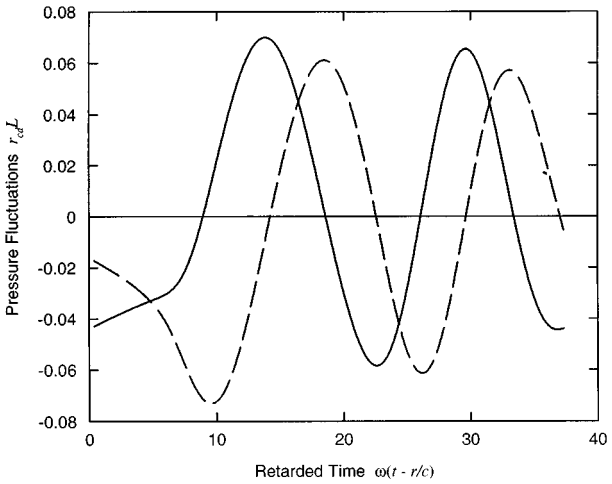

FIG. 19. Time variations of source terms and proposed approximations. $G/\sigma_0=3$, $J=8.64$. ———: $-1.5r_{cd}(0.94\ddot{y}_{c1}-0.34\ddot{y}_{c2})$; – –: $-1.5r_{cd}(0.34\ddot{y}_{c1}+0.94\ddot{y}_{c2})$.

Results shown in Fig. 18 indicate that there exists phase shifts between the source and the longitudinal and transverse acceleration terms. The linear coupling of these accelerations is defined as $L=l_1\ddot{y}_{c1}+l_2\ddot{y}_{c2}$ where l_1 and l_2 are constants. Owing to the phase relationship between the acceleration terms (Fig. 17), these two constants represent a phase shift. Figure 18 illustrates the cases for $l_1=-1$, $l_2=1$ and -1, indicating that source terms $\dddot{S}_i$ and L are nearly in phase. This further confirms the importance of the vortex centroid accelerations in the sound generation process. The time variation of r_cL differs significantly from those of $\dddot{S}_1$ and $\dddot{S}_2$ and thus is not presented. However, the time variation pattern of vortex centroid radius r_c shown in Fig. 15 tends to suggest that r_c can be approximated by the sum of a roughly sinusoidal function r_{cs} and a slowly decreasing function r_{cd}. The amplitude of r_{cs} does not change much with time (not shown here) and thus, due to the decreasing nature of the sound amplitude, it is not believed to be important in the sound generation process. It is expected that r_c will become zero or very small as time approaches infinity and r_{cd} is assumed to take the form of $R_0\exp(-\omega(t-r/c)/b)$. Here, R_0 denotes the initial radial distance of the vortex centroid $(=G/2\sigma_0)$. However, the physical meaning of b is not definitely known. It may represent a certain kind of time scaling but it is more likely a modification factor of the r_c decrease rate. By least-squares method, b is estimated to be 29.2. The time variation of $r_{cd}L$ shows reasonable agreement with the source terms $\dddot{S}_1$ and $\dddot{S}_2$ (Figs. 18 and 19). To correct for the time shift, l_1 and l_2 are estimated to be -0.94 and 0.34, respectively for $\dddot{S}_1$. The corresponding values for $\dddot{S}_2$ are -0.34 and -0.94, respectively. The error for the fitting is around 20% for $\omega(t-r/c)>10$. A similar situation is observed for other values of vorticity provided that coalescence occurs. It is not possible to relate the constants l_1 and l_2 to G/σ_0 as the spatial separation range for the occurrence of coalescence is very narrow. The two vortex cores touch each other at $G/\sigma_0=2$.

The results in this section indicate that the sound from vortex coalescence is mainly related to the longitudinal and transverse accelerating motions of the vortex centroids a short time after the commence of interaction (Figs. 18 and 19). Although an exact agreement in amplitude is not obtained, the fluctuating characteristics of the far-field sound can be explained by the linear coupling between the vortex centroid longitudinal and transverse accelerations.

III. CONCLUSIONS

The sound generated by the pairing of two inviscid finite-core-size equal two-dimensional vortices are studied numerically using the contour dynamics method and vortex sound theory. Two types of pairing, namely the leapfrogging motion and coalescence, are discussed. The sound generation mechanism for each type of pairing is examined in terms of the motions of the vortex centroids as these motions are more easily studied experimentally than those suggested in existing literature.

The sound fields resulted from leapfrogging motion and coalescence are lateral quadrupoles. However, they rotate with a speed different from that of the vortex field. Their directions of rotation follow that of the vortex field for the majority of time. This is different from the results in existing literature on thin core vortex pairing sound study, which indicate that the vortex and the sound fields rotate in the same direction.

In the leapfrogging case, the vortex centroids move in a circular orbit without serious core deformation. The far-field sound is found to consist of two major components—one of low frequency and the other of high frequency. The low-frequency component is generated by the nonlinear couplings of the longitudinal and transverse accelerations of the vortex centroids. The high-frequency component is related to the coupling of the longitudinal and transverse velocities with the radial and angular accelerations of the vortex centroids. The larger the initial separation of the vortex centroids, the more important this high-frequency component becomes. Therefore, the accelerating and decelerating motions of the vortices play an important role in the generation of sound in the leapfrogging case.

The sound generated by vortex coalescence does not contain two components of different frequency as in the leapfrogging case. In general, the spatial separation between the vortex centroids decreases gradually with time. Results suggest that the sound so generated is associated with the longitudinal and transverse accelerations of the vortex centroids and there being no evidence that radial and angular accelerations of these centroids are related to the sound generation process. While linear couplings of vortex centroid longitudinal and transverse accelerations do not give the exact amplitudes of the sound source terms, they show reasonable agreement with the fluctuating characteristics of the sound source strength. The slowly decreasing component of the spatial separation between vortex centroids is also found to be important in controlling the amplitude of the far-field sound.

ACKNOWLEDGMENTS

This work was partly supported by a grant from the Committee of Conference and Research Grant, The University of Hong Kong and by a donation from Dr. Haking Wong.

[1] M. J. Lighthill, ''On sound generated aerodynamically I. General theory,'' Proc. R. Soc. London, Ser. A **211**, 564–587 (1952).
[2] N. Curle, ''The influence of solid boundary upon aerodynamic noise,'' Proc. R. Soc. London, Ser. A **231**, 505–514 (1955).
[3] A. Powell, ''Vortex sound theory,'' J. Acoust. Soc. Am. **36**, 177–195 (1964).
[4] M. S. Howe, ''Contributions to the theory of aerodynamic sound, with application to excess jet noise and the theory of the flute,'' J. Fluid Mech. **71**, 625–673 (1975).
[5] J. E. Bridges and A. K. M. F. Hussain, ''Roles of initial conditions and vortex pairing in jet noise,'' J. Sound Vib. **117**, 289–311 (1987).
[6] M. H. Krane and W. P. Pauley, ''Estimation of the direct acoustic radiation from a transitional boundary layer using velocity measurements,'' J. Sound Vib. **181**, 737–763 (1995).
[7] F. Obermeier and K. Q. Zhu, ''Sound generation by rotor-vortex interaction in low Mach number flow,'' J. Aircraft **30**, 81–87 (1993).
[8] P. A. Lush, ''Measurements of subsonic jet noise and comparison with theory,'' J. Fluid Mech. **46**, 477–500 (1971).
[9] D. G. Crighton, ''Basic principles of aerodynamic noise generation,'' Prog. Aerosp. Sci. **16**, 31–96 (1975).
[10] W. Möhring, ''On vortex sound at low Mach number,'' J. Fluid Mech. **85**, 685–691 (1978).
[11] K. Shariff, A. Leonard, and J. H. Ferziger, ''Dynamics of a class of vortex rings,'' NASA Tech. Memo. **TM-102257** (1989).
[12] S. K. Tang and N. W. M. Ko, ''On sound generated by the interaction of two inviscid vortex rings moving in the same direction,'' J. Sound Vib. **187**, 287–310 (1996).
[13] D. J. Lee and S. O. Koo, ''Numerical study of sound generation due to a spinning vortex pair,'' AIAA J. **33**, 20–26 (1995).
[14] B. E. Mitchell, S. K. Lele, and P. Moin, ''Direct computation of the sound from a compressible corotating vortex pair,'' J. Fluid Mech. **285**, 181–202 (1995).
[15] N. J. Zabusky, M. H. Hughes, and K. V. Roberts, ''Contour dynamics for the Euler equations in two dimensions,'' J. Comput. Phys. **30**, 96–106 (1979).
[16] D. G. Dritschel, ''The nonlinear evolution of rotating configurations of uniform vorticity,'' J. Fluid Mech. **172**, 157–182 (1986).
[17] C. Pozrikidis and J. J. L. Higdon, ''Nonlinear Kelvin-Helmholtz instability of a finite vortex layer,'' J. Fluid Mech. **157**, 225–263 (1985).
[18] J. E. Ffowcs Williams and D. L. Hawkings, ''Shallow water wave generation by unsteady flow,'' J. Fluid Mech. **31**, 779–788 (1968).
[19] H. Ziegler, *Mechanics Vol. 1 Statics of Rigid Bodies, Fluids, and Deformable Solids* (Addison-Wesley, Reading, MA, 1965).
[20] H. Lamb, *Hydrodynamics* (Dover, New York, 1932).
[21] D. G. Dritschel, ''A general theory for two-dimensional vortex interactions,'' J. Fluid Mech. **293**, 269–303 (1995).